ELSEVIER

Physica A 274 (1999) 281–293

PHYSICA A

www.elsevier.com/locate/physa

Applications of statistical mechanics in subcontinuum fluid dynamics

Marek Cieplak[a,*], Joel Koplik[b], Jayanth R. Banavar[c]

[a] *Institute of Physics, Polish Academy of Sciences, 02-668 Warsaw, Poland*

[b] *Benjamin Levich Institute and Department of Physics, City College of New York, NY 10031, USA*

[c] *Department of Physics and Center for Materials Physics, 104 Davey Laboratory, The Pennsylvania State University, University Park, PA 16802, USA*

Abstract

We show results of molecular dynamics studies of fluid flows in the Knudsen regime in which the mean free path is comparable to the system size. We elucidate the boundary conditions at the wall–fluid interface in such flows and find scenarios envisioned by Maxwell. We also find scenarios which do not agree with Maxwell's hypothesis. We focus primarily on the case of repulsive walls and discuss similarities and differences in behavior when the wall–fluid interaction is attractive or repulsive. Striking many body effects are found on increasing the fluid density as one interpolates between the dilute gas and the dense fluid regimes.

PACS: 51.10.+y; 34.10.+x; 92.20.Bk

Novel technological applications often involve flows of rarefied fluids. The density of such fluids may become so low that the description of the flow within the scope of continuum hydrodynamics either breaks down or needs to be supplemented by new parameters. These parameters depend on an atomic level understanding of the phenomena taking place near a confining wall. The interest in such subcontinuum flows goes back to the 19th century studies by Fresnel (1985) and Crookes (1874–1878) of the physics underlying the workings of a radiometer and the phenomena of photophoresis and thermal creep. It also provided motivation for Maxwell to interpret the boundary conditions for fluid in the vicinity of a solid surface [1] from the point of view of his kinetic theory of gases [2]. The 1938 monograph by Kennard [3] gives an exhaustive account of the three basic new phenomena that arise at high dilution: thermal creep, thermal slip, and viscous slip. The latter has been studied by Kundt and Warburg [4],

* Corresponding author.

E-mail address: ciepla@ifpan.edu.pl (M. Cieplak)

0378-4371/99/$ - see front matter
PII: S0378-4371(99)00308-8

Timiriazeff [5], and especially by Knudsen [6,7] after whose name the high dilution regime is called. The Knudsen number, Kn, is defined as a ratio of the mean free path, λ, to the characteristic linear system size, L. At high values of Kn, the flows consist of essentially ballistic movements of molecules between the walls combined with a usually more complex behavior at the walls.

The current return of interest to this classic problem is due to the fact that it is an essential aspect of aerosol dynamics [8,9], high altitude aerodynamics [10], isotope separation schemes [11], and flow cooling techniques [10]. It is also at the core of functioning of micro- and nanoscale mechanical and electromechanical systems [12,13] that are currently being tested and produced as a result of the advances made in silicon-based technology.

Molecular dynamics based simulations offer a unique tool to study subcontinuum aspects of flows in the vicinity of a solid surface [4–19]. At present, there are no other techniques (experimental or theoretical) for deducing the boundary conditions from first principles. Recently [20], we have adopted a fully atomistic model of the fluid *and* of the walls and studied it by molecular dynamics at high and intermediate values of Kn. We have demonstrated that the velocity profiles are very different from those predicted by continuum hydrodynamics and show an unexpected dependence on the density and a distinct dependence on the system size on going from low to high Knudsen numbers. For liquids, an increase in the density results in an increased viscosity and, therefore, in a slowing down of the flow. Strikingly, an opposite tendency is present in the gaseous regime due to an interplay between the interactions of the molecules with the wall and with each other.

In order to elucidate the nature of boundary conditions at a fluid–solid interface, Maxwell [1] has considered two limiting types of the walls: thermal and specular. The latter corresponds to a perfectly smooth surface that would reflect an incident molecule specularly. The former – to a highly uneven or granular surface which would scatter an incident molecule internally and multiply and would eventually reemit it fully thermalized. For the general situation, Maxwell postulated a linear combination of the two kinds of behavior with the weights f for thermal and $(1-f)$ for specular contributions, respectively. This hypothesis has been applied to viscous slip, thermal slip, etc. [3]. Millikan [21], among others, carried out experiments on viscous slip that attempted to unravel Maxwell's linear combination – the effective value of f for common solid and liquids was found to be usually bigger than 0.8 but the determination of f was indirect.

Our own molecular dynamics simulations [20] identified both kinds of limiting behaviors suggested by Maxwell: the collisions with walls were thermal, when there was sufficient attraction between the wall and fluid molecules, or specular, when there was no attractive component in the wall–fluid interactions. However, the crossover between the two behaviors was found to be much more complex and interesting than the simple linear combination envisioned by Maxwell and used by many workers since.

In our previous publication [20], we presented our molecular dynamics results for the case of a wall with strong attraction to the fluid leading to the formation of layers

of fluid atoms next to the wall. This kind of coating provides an efficient thermalizing effect. Here, we focus on the other limiting case and discuss what happens when the wall is purely repulsive. In particular, we demonstrate that the nonmonotonic dependence of the velocity profiles on the density remains qualitatively similar to the attractive wall case. The mechanism for this phenomenon, though still many body in nature, is, however, different. In addition, there are substantial differences in the profiles of density, velocity and shear stress.

An atomic level modelling requires that the fluid and solid molecules be treated on an equal footing. In previous molecular dynamics studies in the Knudsen regime [22,23], it was only the fluid which had an atomic representation and the boundary conditions were put in by hand. As a simplest model, we consider a Lennard–Jones fluid in which two atoms separated by a distance r interact with the potential

$$V_{LJ}(r) = 4\varepsilon \left[\left(\frac{r}{\sigma}\right)^{-12} - \left(\frac{r}{\sigma}\right)^{-6} \right] , \tag{1}$$

where σ is the size of the repulsive core (the potential is truncated at 2.2σ). The flows take place between two solid planar walls parallel to the xy plane with periodic boundary conditions imposed along the x and y directions. Couette flow was generated by moving the walls at constant velocity in opposite directions along the x-axis whereas Poiseuille flow was induced by an application of uniform acceleration g on all the fluid molecules in the x-direction.

As in the paper by Thompson and Robbins [24], we construct the wall from two [001] planes of an fcc lattice. Each wall atom is tethered to a fixed lattice site by a harmonic spring of spring constant k. We chose $k = 400$ so that the mean-square displacement about the lattice sites did not exceed the Lindemann criterion for melting but was close to the value set by this criterion. The wall–fluid interactions were modelled by another Lennard–Jones potential,

$$V_{wf}(r) = 16\varepsilon \left[\left(\frac{r}{\sigma}\right)^{-12} - A \left(\frac{r}{\sigma}\right)^{-6} \right] \tag{2}$$

with the parameter A varying between 1 and 0, corresponding to attractive and repulsive walls, respectively. For the narrowest channel that we studied, the fluid atoms were confined to a space measuring $13.6\sigma \times 5.1\sigma$ in the xy plane and 12.75σ between the walls. We consider a wall which contains 96 wall atoms each (in each wall plane, the atomic periodicity is 0.85σ). The geometry used is illustrated in Fig. 1 which shows a snapshot of the positions of the atoms.

The equations of motion were integrated using a fifth-order Gear predictor-corrector algorithm (see e.g. [25]) with a step size of 0.005τ, where $\tau = (m\sigma^2/\varepsilon)^{1/2}$ and m is the atomic (wall and fluid) mass. The fluid and wall temperatures were fixed at $k_B T/\varepsilon = 1.1$. Here, we present results obtained with the use of Langevin thermostat [26]. We have checked that the results obtained with the use of the Nose–Hoover thermostat [27,28] for the attractive wall case were virtually identical and we expect the same to hold for the repulsive wall as well. The noise was applied in all directions during equilibration and only in the y-direction during the data-taking phase. The averages were obtained

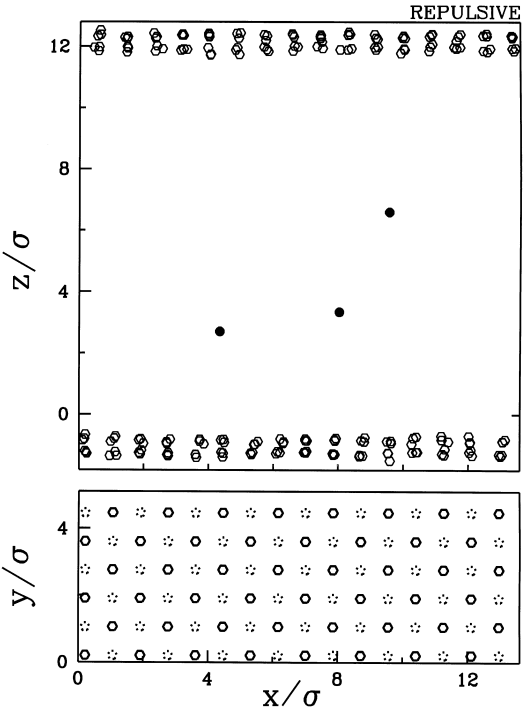

Fig. 1. The snapshot of the 'atoms' of the systems. The black circles represent the fluid atoms. There are three fluid atoms here which illustrates the case of extreme dilution: the central density is $0.004/\sigma^3$. The open hexagons represent the wall atoms. The top panel is the $x-z$ projection whereas the bottom panel is the $x-y$ projection. Here, the hexagons are either solid or dotted to differentiate between atoms from the two wall layers.

over runs which lasted at least 5000 τ, and in the extreme dilution case, for up to 400 000 and 16 000τ for the attractive and repulsive wall cases, respectively. An initial time of at least 400τ was spent for equilibration. The spatial averaging was carried out in slabs of width $\sigma/4$ along the z-axis.

In the dilute gas limit, the Knudsen number, Kn, is defined as λ/L, i.e., as $(\sqrt{2}\pi\rho\sigma^2 L)^{-1}$, where λ is the mean free path, ρ is the fluid number density and L is the characteristic width of the channel. The expression for λ is adopted from the result for the hard core gas. A study of the density profile shows qualitatively different behaviors of the density profiles for the attractive and repulsive walls, as illustrated in Figs. 2 and 3, respectively. In the former case, formation of adsorbed layers form near both walls whereas there is merely a depletion zone, whose thickness is of order σ, alongside the repulsive walls. The first layer at the attractive walls is fairly periodic, as measured by the static structure factor, and the resulting local order corresponds to a square lattice. L is defined as an effective channel width in which the flow takes place (in the attractive case this is the distance between centers of the second layers and in the

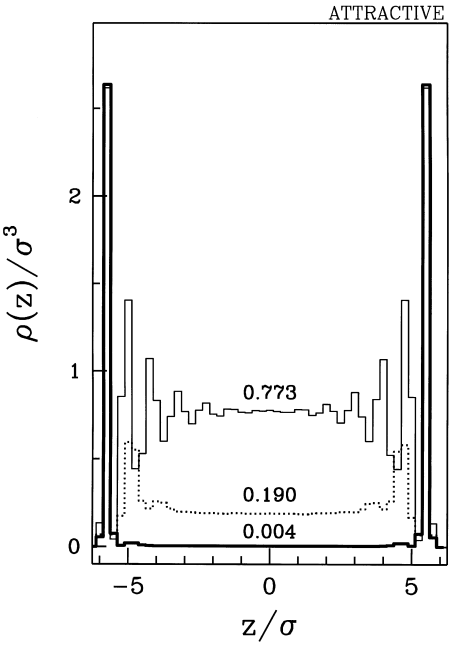

Fig. 2. The density profiles for the attractive wall and for the three densities indicated. The values refer to the density in the central region.

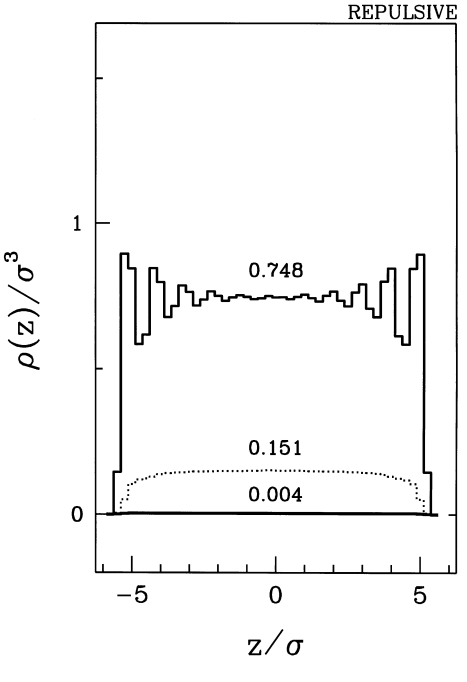

Fig. 3. The density profiles for the repulsive wall.

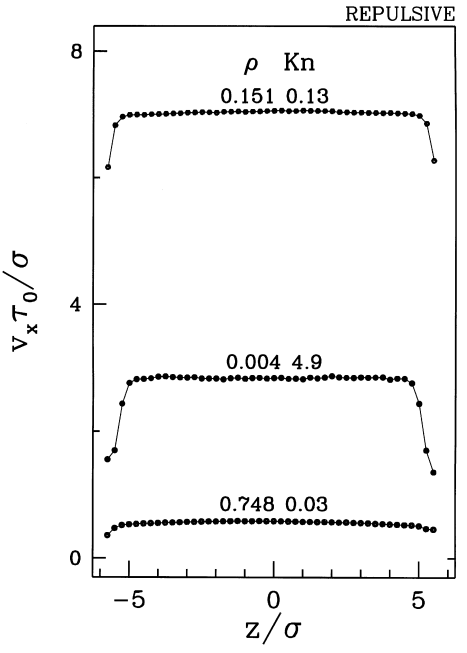

Fig. 4. Velocity profiles of gravity-driven channel flow with $g = 0.01\sigma/\tau^2$ for the smallest width channel with repulsive walls. The values of the interior fluid density and the corresponding Knudsen number are indicated. The inner wall layers are at the edges of the figure.

repulsive case this is the width of a region in which the density is non-zero). In the center of the channel, the fluid density is essentially constant and this value is chosen as ρ in the definition of Kn. Increasing the density to liquid values results, for both kinds of walls, in a buildup of atomic layers further and further into the bulk.

Fig. 4 shows the flow velocity profiles for three different values of ρ (or Kn) for the repulsive wall case. The flow was induced by a small gravitational force with $g = 0.01$ along the x-axis. The profiles correspond to plug flows across the whole density range with some Poiseuille-like parabolicity present only at the highest densities. This is in contrast to the profiles found for the attractive wall case [20]. For the attractive walls, the profiles are plug-flow like only at high dilution whereas they are nicely parabolic at intermediate and high densities. The attractive wall exerts a pull on the fluid molecules leading to virtually no-slip boundary conditions whereas the repulsive wall gives rise to a large slip.

A further understanding of the problem is obtained by studying the shear stress component of the stress tensor. This is shown in Figs. 5 and 6 for the attractive and repulsive walls, respectively. In the attractive case, ρ of 0.004 corresponds to a very small velocity gradient and thence virtually zero stress. At intermediate and high densities, however, the shear stress has an overall slope indicating a non-zero viscosity. In the repulsive case, the behavior is similar but the shear stress is an order

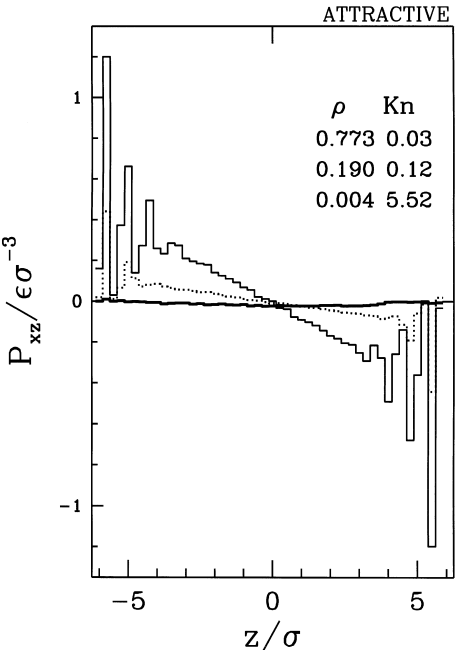

Fig. 5. The shear stress profiles of the gravity-driven channel flow for the smallest width channel with attractive walls. The values of the interior fluid density and the corresponding Knudsen number are indicated and they are ordered top to bottom corresponding to the left-hand side portions of the profiles.

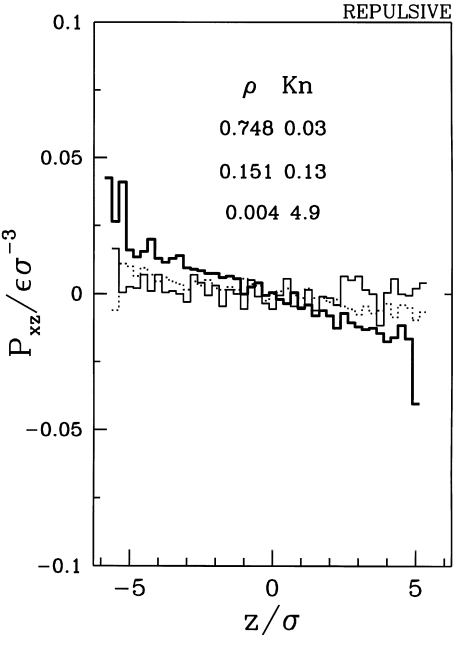

Fig. 6. Same as in Fig. 5 but for the repulsive walls.

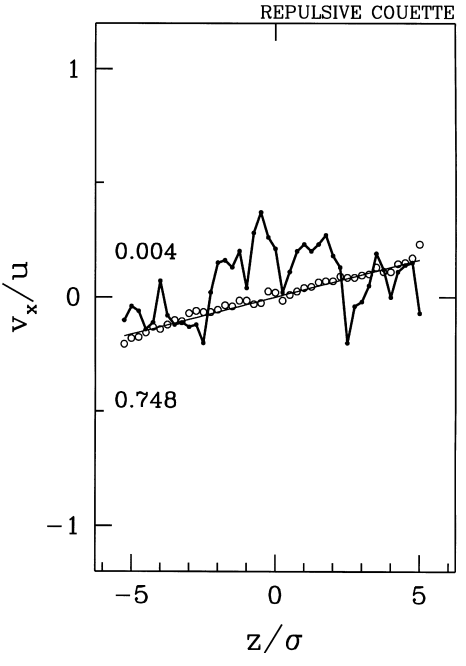

Fig. 7. Velocity profiles of Couette flow with $u = 0.1\sigma/\tau$ for the smallest width channel with repulsive walls. The fluid densities in the central region are indicated.

of magnitude smaller. The decoupling of the fluid flow from the repulsive wall is also seen in Couette flow. This is illustrated in Fig. 7 which shows the velocity profile for the situation in which the top wall moves to the right and the bottom wall moves to the left, both with a speed of u. In the limit of large dilution, the profile is not smooth. The smoothness observed in gravity-driven flow is due to an organizing influence of the gravitational force which acts on all molecules. In Couette flow, the forcing is restricted to the wall area and, in the absence of viscous effects, it does not propagate inward to provide organization.

We now proceed to study the effect of interactions between the fluid particles undergoing gravity-driven channel flow on varying ρ within the channel. In such a flow, the velocity field is the highest in the middle of the channel and is denoted by $v_{\max}$. For the attractive wall, one expects that $v_{\max}$ ought to scale as L at small densities and as L^2 at high densities. The low density behavior is implicit in an analytic result for the flowrate derived by Smoluchowski [29,3] and its physical origin is that the driving force is effective in accelerating the fluid particles only during the time spent traversing the channel between collisions with the walls (and the associated adsorbed layers). This time simply scales as the channel width. The high density behavior follows from the Navier–Stokes equation with no-slip boundary conditions. The crossover between the two situations results in a monotonic dependence of $v_{\max}$ on ρ – there is a maximum around a characteristic density ρ_K of about $0.19\sigma^{-3}$ above which the velocity profiles

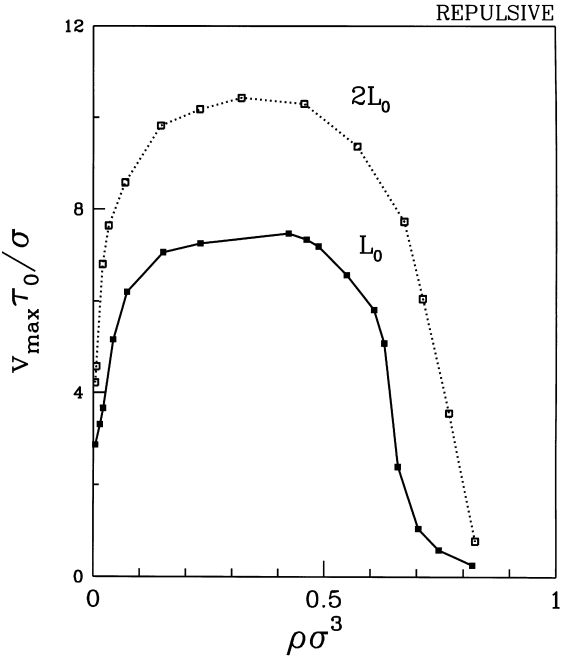

Fig. 8. Plot of the fluid velocity in the middle of the channel in gravity-driven flow with $g = 0.01\tau/\sigma^2$ as a function of fluid density The plot is for two different channel widths. The L_0 in the figure denotes the narrowest channel. $2L_0$ denotes a channel that is effectively twice as wide as the smallest channel.

are clearly parabolic [20]. Above ρ_K, the fluid intermolecular interactions dominate the influence of the wall.

Fig. 8 shows that the repulsive wall also generates a maximum in the dependence of $v_{\max}$ on ρ at ρ_K of about $0.4\sigma^{-3}$. However, the scaling behavior appears different. Doubling the separation between the walls at the highest Knudsen numbers results in increasing $v_{\max}$ only by a factor of about $\frac{3}{2}$. A similar factor characterizes the scaling around ρ_K. A further increase in ρ makes the scaling factor bigger (between 3 and 6) with no evidence for the quadratic law. The low density behavior should be related to the fact that the saturation of the velocity profile with time is not due to the thermalization at the wall but merely due to bulk thermalization by the Langevin noise. Furthermore, the wider the channel, the longer lasting is the accelerating influence of the force. The large density behavior, on the other hand, is modified by the large slip length. A further increase in the wall-to-wall separation is expected to lead to the L^2 law asymptotically.

The most interesting aspect of Fig. 8 is that, as in the attractive wall case, $v_{\max}$ increases with ρ when $\rho < \rho_K$. In the attractive wall case we attributed this phenomenon to an increased scattering which keeps the atoms in the channel longer [20]. This results in two effects: (1) the acceleration time gets extended and (2) the time spent on thermalization at the walls gets reduced. A scattering-induced effective deflection of

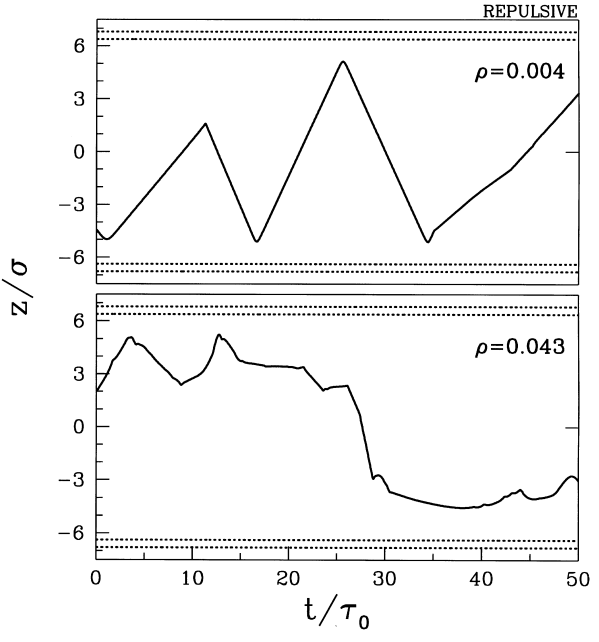

Fig. 9. Plots of the time dependence of the z-coordinate of a typical fluid particle undergoing gravity-driven flow in the narrowest channel. The horizontal dotted lines indicate the z-coordinates of the wall molecules.

ballistic trajectories from the wall is also present in the case of the repulsive wall and is illustrated in Fig. 9. In this case, however, only the first of the above two effects is operational since the specularly reflecting wall has little thermalizing influence. The upper panel of Fig. 9 shows the trajectory of the z-coordinate of a typical atom when three fluid atoms are present in the channel. At the wall, the atom is reflected approximately specularly and moves out of the vicinity of the wall immediately. The bottom panel shows qualitatively different behavior when 27 more atoms are added into the system: each atom hits the wall less frequently.

A useful characterization of the fluid–solid interface is provided by the collision kernel [30,31] – the probability density that a molecule striking the surface with a given velocity reemerges with a specific velocity after a given residence time. We find that, both for the attractive and repulsive walls, the scenarios envisioned by Maxwell hold very well. For the repulsive wall, the residence time is negligible and the reflections are specular. On the other hand, for the attractive walls the distribution of residence times develops a long tail and the residence time is found to be uncorrelated with the outgoing velocity. Strikingly, the velocity distribution of a particle after the collision with the wall is substantially independent of the incoming velocity. The velocity distributions agree with the thermal wall scenario and for v_x and v_z they are given by [2,3,32]

$$\phi_x(v_x) = \sqrt{\frac{m}{2\pi k_B T}} \exp\left(-\frac{m v_x^2}{2 k_B T}\right) , \tag{3}$$

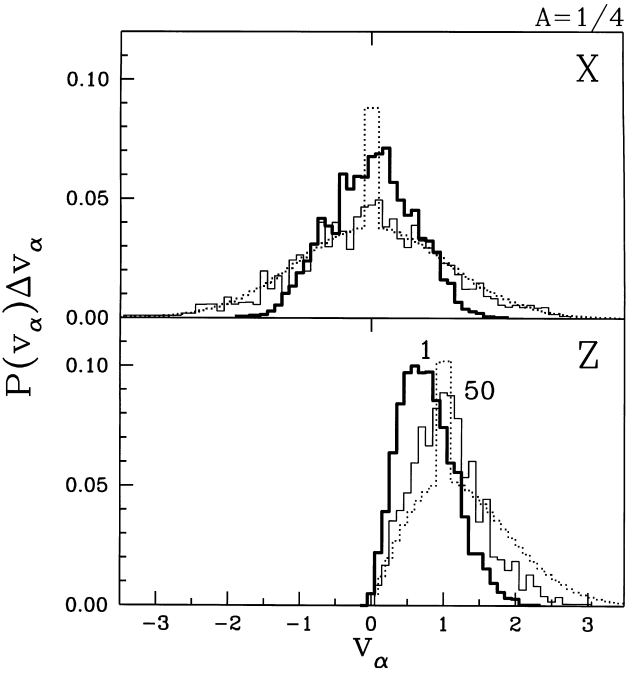

Fig. 10. The thick solid lines (marked additionally by the label 1) represent the probability density distributions for the velocity components of the outgoing velocity of a fluid molecule after collision with a wall with the wall–fluid interactions given by Eq. (2) with $A=\frac{1}{4}$. There are no adsorbed fluid atoms on the wall. The upper and lower panels are for the x and z (normal) velocity components, respectively. The statistics are based on about 3000 scattering events with the wall. The dotted lines correspond to the linear combination of to the combined distributions $f\phi_\alpha(v_\alpha)+(1-f)\delta(v_\alpha-v_\alpha^{sp})$ with $f=0.9$. Here, ϕ_α is given by Eqs. (3) and (4) and v_α^{sp} denotes the specularly reflected component of the velocity. The selected value of f offers the closest match to the data for both velocity components simultaneously. The thinner solid lines in the main panel (marked by the label 50) represent the velocity distributions obtained for $A=\frac{1}{4}$ when 50 fluid molecules are placed in the narrowest channel ($\rho=0.066$).

and

$$\phi_z(v_z)=\frac{m}{k_BT}v_z\exp\left(-\frac{mv_z^2}{2k_BT}\right)\ , \tag{4}$$

respectively.

Following Ref. [20], we now consider the case in which the wall–fluid potential is given by Eq. (2) with $A=\frac{1}{4}$. This corresponds to the crossover behavior from that of specular reflection to that of a thermal wall. Fig. 10 shows that, in this case, the velocity distributions of the scattered particles clearly deviate from pure thermal behavior and contains a specular component. However, the resulting distributions are more complex than the simple linear combination form.

The behavior of the collision kernel is further enriched on considering the role of the interactions between the fluid molecules as the Knudsen number decreases to a value of 0.27 corresponding to a density of $\rho=0.066$. The density profile corresponding to this

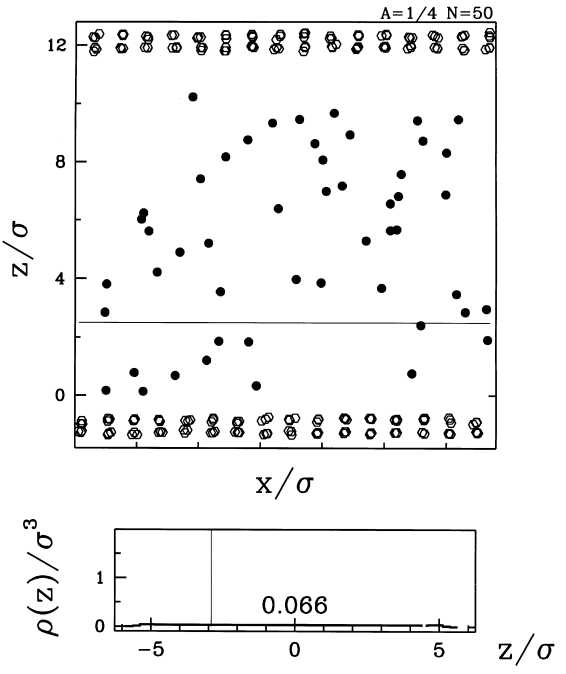

Fig. 11. The top panel shows a snapshot of the atoms, similar to Fig. 1, which depicts the geometry used to determine the effect of other molecules on the effective collision kernel for one molecule. There are 50 fluid molecules here and $A = \frac{1}{4}$. The thin horizontal line corresponds to the monitoring plane. The bottom panel shows the corresponding density profile. The value of the density at the center is indicated.

situation is shown in the bottom panel of Fig. 11 whereas a corresponding snapshot is shown in the top panel of this figure. The distributions are obtained by monitoring molecules incident on the walls at a distance of 1 mean free path (or 3.4σ) from the walls, marked by a line in Fig. 11, during the evolution of the system. The data were obtained based on about 1100 events in which the incoming molecules happened to be moving nearly normally towards one of the walls with a speed between 0.8 and $1.2\sigma/\tau_0$ and then reemerged with velocities distributed as shown in the figure. The influence of other fluid molecules is seen to lead to the distributions more closely approaching the thermal ones. Moving the monitoring plane further away from the wall also results in bringing the distributions closer to the thermal ones.

The nature of the boundary conditions at a fluid–solid interface is thus more complex than those envisioned by Maxwell and molecular dynamics simulations are a useful tool to understand this complexity.

We are indebted to Mark Robbins and Riina Tehver for many valuable discussions. This work was supported by KBN (Grant No. 2P03B-025-13), NASA, and the Petroleum Research Fund administered by the American Chemical Society.

References

[1] J.C. Maxwell, Philos. Trans. R. Soc. Lon. Ser. A 170 (1867) 231.
[2] J.C. Maxwell, Philos. Mag. 19 (1860) 20.
[3] E.H. Kennard, Kinetic Theory of Gases, McGraw-Hill, New York, 1938.
[4] A. Kundt, E. Warburg, Philos. Mag. 50 (1875) 53.
[5] A.K. Timiriazeff, Ann. Phys. 40 (1913) 971.
[6] M. Knudsen, Ann. Phys. 28 (1909) 75.
[7] M. Knudsen, Ann. Phys. 48 (1915) 1113.
[8] W.H. Marlow (Ed.), Aerosols: Aerosol Microphysics I – Particle Interactions, Springer, New York, 1980.
[9] J.H. Seinfeld, S.N. Pandis, Atmospheric Chemistry and Physics, Wiley, New York, 1998.
[10] E.P. Muntz, D. Weaver, D. Campbell (Eds.), Rarified Gas Dynamics, American Institute of Aeronautics and Astronautics, Washington, 1989.
[11] W. Ehrfeld, Elements of Flow and Diffusion Processes in Separation Nozzles, Springer, New York, 1983.
[12] C.-J. Kim, (Ed.), Microelectromechanical systems (MEMS), American Society of Mechanical Engineers, New York, 1997.
[13] C.-M. Ho, Y.-C. Tai, Ann. Rev. Fluid Mech. 30 (1998) 579.
[14] J. Koplik, J.R. Banavar, Comput. Phys. 12 (1998) 424.
[15] J. Koplik, J.R. Banavar, Annu. Rev. Fluid Mech. 27 (1995) 257–292.
[16] S. Sugano, Microcluster Physics, Springer, Berlin, 1991.
[17] B. Bhushan, J.N. Israelachvili, U. Landman, Nature 374 (1995) 607.
[18] I. Bitsanis, T.K. Vanderlick, M. Tirrel, H.T. Davis, J. Chem. Phys. 89 (1988) 3252.
[19] W. Loose, S. Hess, Rheol. Acta 28 (1989) 91.
[20] M. Cieplak, J. Koplik, J.R. Banavar, submitted for publication.
[21] R.A. Millikan, Phys. Rev. 21 (1923) 217.
[22] D.K. Bhattacharya, G.C. Lie, Phys. Rev. A 43 (1991) 761.
[23] D.L. Morris, L. Hannon, A.L. Garcia, Phys. Rev. A 46 (1992) 5279.
[24] P.A. Thompson, M.O. Robbins, Phys. Rev. A 41 (1990) 6830.
[25] M.P. Allen, D.J. Tildesley, Computer Simulation of Liquids, Clarendon Press, Oxford, 1987.
[26] G.S. Grest, K. Kremer, Phys. Rev. A 33 (1986) 3628.
[27] S. Nose, Mol. Phys. 52 (1984) 255.
[28] W.G. Hoover, Phys. Rev. A 31 (1985) 1695.
[29] M. Smoluchowski, Ann. Phys. 33 (1910) 1559.
[30] C. Cercignani, The Boltzmann Equation and its Applications, Springer, Berlin, 1988.
[31] Y. Matsumoto, N. Yamanishi, H. Shobatake, Proceedings of the 19th International Symposium on Rarefied Gas Dynamics, Vol. 995, 1994.
[32] R. Tehver, F. Toigo, J. Koplik, J.R. Banavar, Phys. Rev. E 57 (1998) R17.